

Discovery of interstellar 3-cyano propargyl radical, CH₂CCCN [★]

C. Cabezas¹, M. Agúndez¹, N. Marcelino^{2,3}, B. Tercero^{2,3}, J. R. Pardo¹, P. de Vicente³ and J. Cernicharo¹

¹ Grupo de Astrofísica Molecular, Instituto de Física Fundamental (IFF-CSIC), C/ Serrano 121, 28006 Madrid, Spain. e-mail: carlos.cabezas@csic.es; jose.cernicharo@csic.es

² Observatorio Astronómico Nacional (IGN), C/ Alfonso XII, 3, 28014, Madrid, Spain.

³ Centro de Desarrollos Tecnológicos, Observatorio de Yebes (IGN), 19141 Yebes, Guadalajara, Spain.

Received; accepted

ABSTRACT

We report the first detection in interstellar space of the 3-cyano propargyl radical (CH₂C₃N). This species was observed in the cold dark cloud TMC-1 using the Yebes 40m telescope. A total of seven rotational transitions for both ortho- and para-CH₂C₃N species were observed in the 31.0-50.4 GHz range. We derive a total column density of $(1.6\pm 0.4)\times 10^{11}$ cm⁻² and an ortho/para ratio of 2.4 ± 1.2 , which implies an abundance ratio CH₂C₃N/CH₃C₃N ~ 0.1 , in sharp contrast with the smaller analogues, in which case CH₂CN/CH₃CN ~ 3 . This indicates that the chemistry of the cyanides CH₂C₃N and CH₃C₃N behaves differently to that of the smaller analogues CH₂CN and CH₃CN. According to our chemical model calculations, the radical CH₂C₃N is mostly formed through the neutral-neutral reactions C + CH₂CHCN, C₂ + CH₃CN, and CN + CH₂CCH together with the dissociative recombination of the CH₃C₃NH⁺ ion with electrons. The neutral-neutral reaction N + C₄H₃ could also lead to CH₂C₃N, although its role is highly uncertain. The identified radical CH₂C₃N could play a role in the synthesis of large organic N-bearing molecules, such as benzonitrile (c-C₆H₅CN) or nitrogen heterocycles.

Key words. Astrochemistry — ISM: molecules — ISM: individual (TMC-1) — line: identification — molecular data

1. Introduction

Cold dark clouds such as TMC-1 present a rich and complex chemistry that leads to the formation of a great variety of molecules. The list of molecular species observed in these clouds includes cations, mostly protonated forms of closed-shell abundant molecules (e.g. Agúndez et al. 2015; Marcelino et al. 2020; Cernicharo et al. 2020a, 2021a,b), and some hydrocarbon and nitrile anions (e.g. Cernicharo et al. 2020b), although most of the detected species are electrically neutral. Closed-shell species constitute only one-third of the neutral species observed in cold dark clouds, but they are the most abundant ones. The remaining two-thirds of the neutral species detected in these cold environments are open-shell radicals. Apart from OH, CH, C₂H, C₄H, C₆H, CH₂CCH, and NO, observed radicals have low abundances because, as ions, they are highly reactive species (see e.g. Agúndez & Wakelam 2013). Another fact that complicates the detection of radicals is the spectral dilution resulting from line splitting due to the interaction of the rotational angular momentum with different types of angular momenta, such as the electronic orbital, the electron spin, or the nuclear spin.

Cyanomethyl radical, CH₂CN, is the simplest member of the CH₂C_nN ($n\geq 1$) radical series. It is derived from the closed-shell species CH₃CN by removing one hydrogen atom. CH₂CN was detected in the cold dark cloud TMC-1 by Saito et al. (1988) and Irvine et al. (1988). Recent observations of TMC-1 using the QUIJOTE¹ line survey (Cernicharo et al. 2021c) show that

CH₂CN is a fairly abundant radical with a CH₂CN/CH₃CN ratio of 3.2 ± 0.4 . (Cabezas et al. 2021a). Hence, it is expected that larger members of the CH₂C_nN series can be observed in this source as well. CH₂CCN is the next member of the series. This radical is known as α -cyanovinyl radical, and it has been characterized experimentally. Its rotational spectrum in the centimetre and millimetre regions has been observed (Tang et al. 2000; Seiki et al. 2000; Prozument et al. 2013), as has its Fourier-transform infrared emission spectrum (Letendre & Dai 2002). However, the data available in the literature do not allow the precise predictions needed to search for it in the interstellar medium (ISM) to be obtained, and its astronomical detection has not been claimed so far.

The largest member of the CH₂C_nN radical series that has been characterized in the laboratory is the 3-cyano propargyl radical, CH₂C₃N (see Fig. 1). Chen et al. (1998) detected the ortho-CH₂C₃N using Fourier transform microwave spectroscopy, and three years later Tang et al. (2001) improved the rotational parameters for CH₂C₃N by observing lines for the para-CH₂C₃N species using the same spectroscopy technique. Chen et al. (1998) also reported on their astronomical search for the CH₂C₃N radical, which they carried out using their experimental data. The obtained upper limit allowed them to estimate a column density of 2×10^{11} cm⁻² in TMC-1.

In this letter we report the first identification of the CH₂C₃N radical in space towards TMC-1, based on the laboratory data previously reported by Chen et al. (1998) and Tang et al. (2001). The derived column density for this radical is compared with analogue radicals and closed-shell species and is interpreted via chemical models to understand the chemical processes in which it is involved.

[★] Based on observations carried out with the Yebes 40m telescope (projects 19A003, 20A014, and 20D15). The 40m radio telescope at Yebes Observatory is operated by the Spanish Geographic Institute (IGN, Ministerio de Transportes, Movilidad y Agenda Urbana).

¹ Q-band Ultrasensitive Inspection Journey to the Obscure TMC-1 Environment

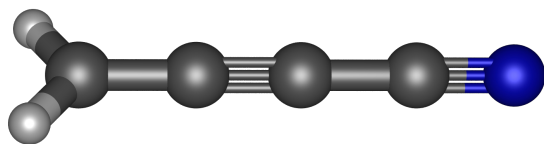


Fig. 1. Molecular structure of the $\text{CH}_2\text{C}_3\text{N}$ radical.

2. Observations

The data presented in this work are part of the QUIJOTE spectral line survey in the Q band towards TMC-1 ($\alpha_{J2000} = 4^{\text{h}}41^{\text{m}}41.9^{\text{s}}$ and $\delta_{J2000} = +25^{\circ}41'27.0''$) that was performed at the Yebes 40m radio telescope during various observing sessions between November 2019 and April 2021. A total of 30 new molecular species have been detected using this survey (Cernicharo et al. 2020a,b,c; Marcelino et al. 2020, 2021; Agúndez et al. 2021a,b; Cabezas et al. 2021a,b,c; Cernicharo et al. 2021a,b,c,d,e,f,g,h). All observations were carried out using the frequency switching technique (Cernicharo et al. 2019), with a frequency throw of 10 MHz during the two first observing runs and of 8 MHz in the later ones. This observing mode provides a S/N that is $\sqrt{2}$ higher than the unfolded data, but on the other hand it produces negative spectral features at ± 10 MHz or 8 MHz of each rotational transition. These negative features can be easily identified because of their symmetric displacement by exactly the frequency throw. As shown in Fig. 2, we blanked these channels with negative features for the sake of convenience. The selected temperature scale is T_A^* . The T_{MB} can easily be obtained by dividing the observed T_A^* by the beam efficiency. Values of η_{MB} have been provided by Tercero et al. (2021). The T_A^* was calibrated using two absorbers at different temperatures and the atmospheric transmission model ATM (Cernicharo 1985; Pardo et al. 2001).

Different frequency coverages were observed, 31.08-49.52 GHz and 31.98-50.42 GHz, which permitted us to verify that no spurious ghosts were produced in the down-conversion chain. In this chain the signal coming from the receiver is down-converted to 1-19.5 GHz and then split into eight bands with a coverage of 2.5 GHz, each of which is analysed by the fast Fourier transform (FFT) spectrometers. Calibration uncertainties were adopted to be 10 %, based on the observed repeatability of the line intensities between different observing runs. All data were analysed using the GILDAS package².

3. Results

The 3-cyano propargyl radical, $\text{CH}_2\text{C}_3\text{N}$, is an asymmetric top molecule (see Fig. 1) with a doublet electronic ground state (2B_1) and a fairly large dipole moment of 4.43 D (Tang et al. 2001). Due to its molecular symmetry, C_{2v} , it is necessary to discern between ortho- $\text{CH}_2\text{C}_3\text{N}$ and para- $\text{CH}_2\text{C}_3\text{N}$ levels, which are described by K_a even and K_a odd, respectively. Chen et al. (1998) observed in the laboratory four rotational transitions with $K_a = 0$ for ortho- $\text{CH}_2\text{C}_3\text{N}$. A total of 89 hyperfine components were analysed with an effective Hamiltonian for a linear molecule in a $^2\Sigma$ electronic state, and a set of linear-molecule-like constants was determined. These constants can only be used to predict the rotational transitions for ortho- $\text{CH}_2\text{C}_3\text{N}$ in a hypothetical astronomical search. Tang et al. (2001) confirmed the C_{2v} structure for $\text{CH}_2\text{C}_3\text{N}$ by measuring and analysing both $K_a = 1$ for para- $\text{CH}_2\text{C}_3\text{N}$ and those transitions previously measured

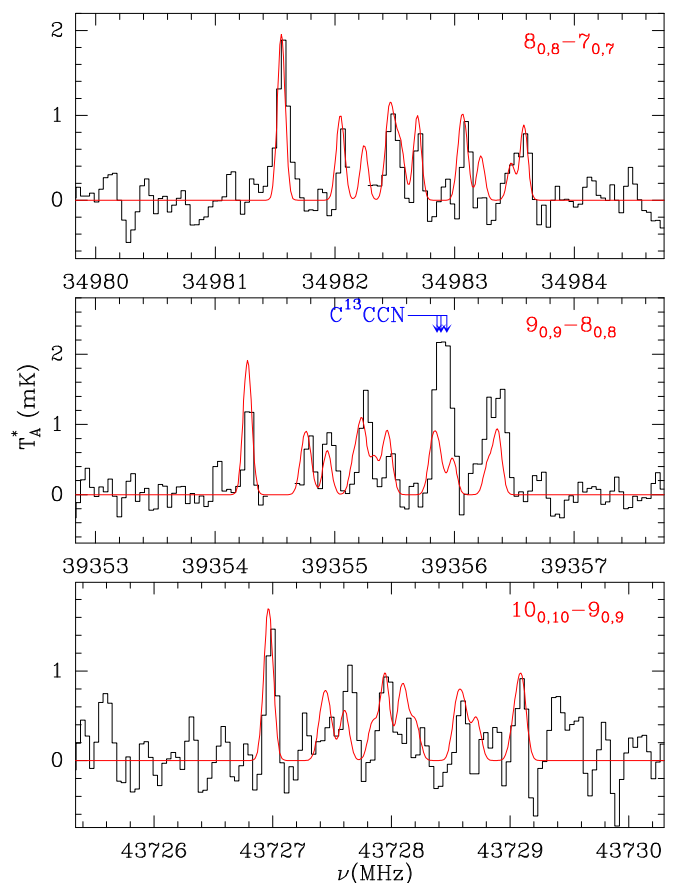


Fig. 2. Observed $N_{K_a, K_c} = 8_{0,8}-7_{0,7}$, $9_{0,9}-8_{0,8}$, and $10_{0,10}-9_{0,9}$ lines of ortho- $\text{CH}_2\text{C}_3\text{N}$ in TMC-1 in the 31.0-50.4 GHz range. The most intense hyperfine components for each rotational transition are shown. The abscissa corresponds to the rest frequency, assuming a local standard of rest velocity of 5.83 km s^{-1} . Blanked channels correspond to negative features produced in the folding of the frequency switching data. The ordinate is antenna temperature in millikelvins. Curves shown in red are the computed synthetic spectra.

by Chen et al. (1998) with $K_a = 0$ for ortho- $\text{CH}_2\text{C}_3\text{N}$. In this manner, Tang et al. (2001) determined a total of 15 molecular constants for the asymmetric-rotor $\text{CH}_2\text{C}_3\text{N}$ radical, which properly describe the rotational spectrum of this species and allow its radio-astronomical search, since both ortho- and para- $\text{CH}_2\text{C}_3\text{N}$ are observable in the ISM.

Based only on the experimental data reported by Chen et al. (1998), W. D. Langer & T. Velusamy (cited as private communication in Chen et al. 1998) searched for ortho- $\text{CH}_2\text{C}_3\text{N}$ in TMC-1. An upper limit of $T_A^* \leq 5 \text{ mK}$ for the $N = 5-4$ transition at 21,864 MHz, averaged over the 0.20 km s^{-1} spectral resolution, was obtained using the position switching observing mode with an on-source integration time of 6 hr. From these observations, W. D. Langer & T. Velusamy estimate that the column density of $\text{CH}_2\text{C}_3\text{N}$ in TMC-1 is $\leq 2 \times 10^{11} \text{ cm}^{-2}$ for an assumed dipole moment of 4.42 D, a rotational temperature of 10 K, a line width of 0.5 km s^{-1} , and under the assumption that the source fills the telescope beam, $45''$. Our QUIJOTE survey has an excellent sensitivity, with a T_A^* rms noise level of 0.30 mK per 38.15 kHz channel, which has allowed the detection of the 3-cyano propargyl radical.

Our search for $\text{CH}_2\text{C}_3\text{N}$ is based on the frequency predictions for the ortho and para species made using the laboratory data from Chen et al. (1998) and Tang et al. (2001). These

² <http://www.iram.fr/IRAMFR/GILDAS>

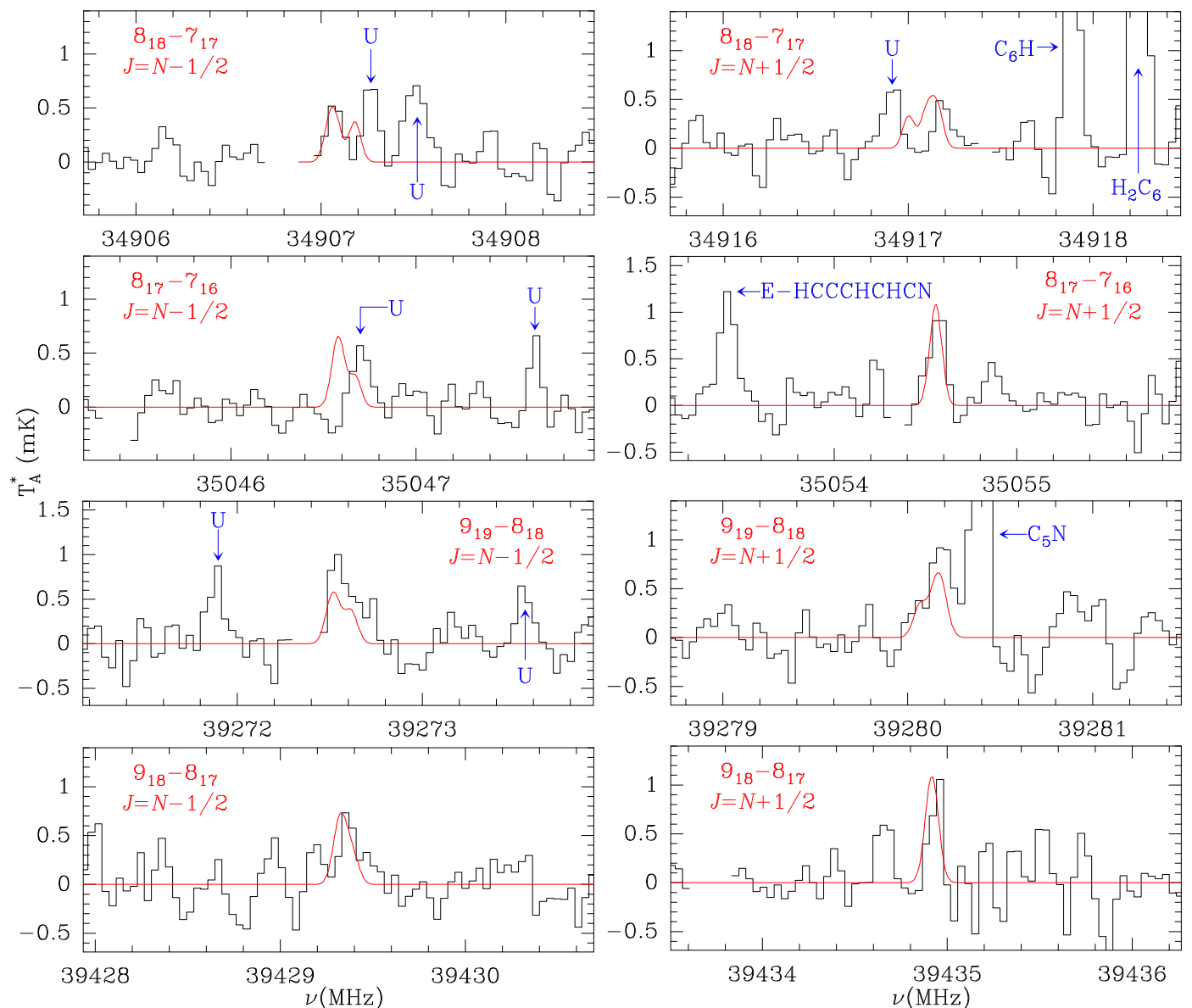


Fig. 3. Observed rotational transitions of para-CH₂C₃N in TMC-1 in the 31.0-50.4 GHz range. The most intense hyperfine components for each rotational transition are shown. The abscissa corresponds to the rest frequency, assuming a local standard of rest velocity of 5.83 km s⁻¹. The ordinate is antenna temperature in millikelvins. Curves shown in red are the computed synthetic spectra.

predictions are available in the CDMS catalogue (Müller et al. 2005), entry number 064509, together with other data, such as partition functions. They were implemented in the MADEX code (Cernicharo 2012) to compute column densities. We considered the ortho and para species separately as there are no radiative or collisional transitions between them. The lowest energy level of the para species ($1_{1,1}$) is 13.9 K above the ortho ground level ($0_{0,0}$). We adopted a dipole moment of 4.43 D, as calculated by Tang et al. (2001).

Four transitions of ortho-CH₂C₃N with $K_a = 0$ are covered by our QUIJOTE survey, at 34.9, 39.3, 43.7, and 48.1 GHz. We observed three groups of lines at the predicted frequencies of the transitions $8_{0,8}-7_{0,7}$, $9_{0,9}-8_{0,8}$, and $10_{0,10}-9_{0,9}$. Figure 2 shows the lines corresponding to these rotational transitions of ortho-CH₂C₃N with their hyperfine structure, as observed in TMC-1. Our model predicts an intensity of 1.0 mK for the strongest hyperfine component of the $11_{0,11}-10_{0,10}$ transition and between 0.4-0.7 mK for the others. None of these lines are detected at

the 3σ (0.9 mK) detection limit of the survey at this frequency. All the hyperfine components are detected with antenna temperatures between 0.6 and 1.9 mK, and a few of them are blended with negative features produced in the folding of the frequency switching data (i.e. for the $8_{0,8}-7_{0,7}$ transition). The hyperfine components of ortho-CH₂C₃N are precisely centred at the calculated frequencies with deviations in frequency smaller than 20 kHz, which is within the uncertainty given by the spectral resolution of 38.15 kHz and the error in the Gaussian fit.

A total of eight rotational transitions of para-CH₂C₃N with $K_a = 1$ are covered by our survey. However, those with an N quantum number higher than 9 are predicted at frequencies that are not detectable with the sensitivity of our survey. The spectral pattern of the $K_a = 1$ transitions of para-CH₂C₃N is very different to that of the $K_a = 0$ lines, where all the hyperfine components are spread over 2.0-2.5 MHz. In contrast, each $K_a = 1$ line is formed by two groups of hyperfine components separated by a few megahertz due to the spin-doubling interactions. This

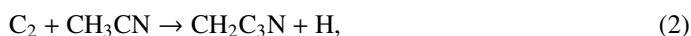
separation decreases with the N quantum number. This is illustrated in Fig. 3, where we show the four rotational transitions of para- $\text{CH}_2\text{C}_3\text{N}$ with $K_a = 1$ observed in our survey. Six groups of lines are clearly detected with a maximum antenna temperature of 0.6 mK. The other two, $8_{1,8}-7_{1,7}$ with $J = N + 1/2$ and $8_{1,8}-7_{1,6}$ with $J = N - 1/2$, are affected by negative features produced in the folding of the frequency switching data and thus cannot be confirmed.

An analysis of the observed intensities using a line profile fitting method (Cernicharo et al. 2021a) provides a rotational temperature of 7 ± 1 K, while the observed intensities are reproduced with column densities of $(1.1 \pm 0.3) \times 10^{11} \text{ cm}^{-2}$ and $(4.6 \pm 1.1) \times 10^{10} \text{ cm}^{-2}$ for ortho- and para- $\text{CH}_2\text{C}_3\text{N}$, respectively. The ortho/para ratio found is 2.4 ± 1.2 . Chen et al. (1998) reported an estimated column density for $\text{CH}_2\text{C}_3\text{N}$ in TMC-1 $\leq 2 \times 10^{11} \text{ cm}^{-2}$, which is in accordance with our value for the total (ortho plus para) column density for $\text{CH}_2\text{C}_3\text{N}$ of $(1.6 \pm 0.4) \times 10^{11} \text{ cm}^{-2}$.

4. Chemical modelling

To examine the chemical processes that could form the radical $\text{CH}_2\text{C}_3\text{N}$ in TMC-1, we carried out chemical modelling calculations. We adopted typical conditions of cold dark clouds: a gas kinetic temperature of 10 K, a volume density of H nuclei of $2 \times 10^4 \text{ cm}^{-3}$, a cosmic-ray ionization rate of H_2 of $1.3 \times 10^{-17} \text{ s}^{-1}$, a visual extinction of 30 mag, and low-metal elemental abundances (see e.g. Agúndez & Wakelam 2013). We used the chemical network RATE12 from the UMIST database (McElroy et al. 2013), with updates from Loison et al. (2014) and Marcelino et al. (2021) to include $\text{C}_4\text{H}_3\text{N}$ isomers.

Since the radical $\text{CH}_2\text{C}_3\text{N}$ is not included in the UMIST database, we added some reactions to account for its formation and destruction. We assumed that $\text{CH}_2\text{C}_3\text{N}$ is destroyed through reactions with the neutral atoms C, N, and O, as well as through reactions with the atomic cations C^+ and H^+ , with rate coefficients similar to those involving the radical CH_2CN . As formation routes, we included the reactions



Reaction (1) has been studied using crossed molecular beam experiments and theoretical calculations (Su et al. 2005; Guo et al. 2006a). These studies indicate that the reaction is barrier-less and occurs through H atom elimination, yielding as main products the radicals 1-cyano propargyl (HCCCHCN) and 3-cyano propargyl ($\text{CH}_2\text{C}_3\text{N}$). The latter is inferred to be produced at least twice less efficiently than the former (Guo et al. 2006a), and we thus adopted a rate coefficient of $10^{-10} \text{ cm}^3 \text{ s}^{-1}$ for reaction (1). Reaction (2) has not been studied to our knowledge, but some information can be extracted from the known reactivity of C_2 with unsaturated hydrocarbons, in particular with CH_3CCH . The reaction $\text{C}_2 + \text{CH}_3\text{CCH}$ has been measured to be rapid, with a nearly constant rate coefficient of $(4-5) \times 10^{-10} \text{ cm}^3$

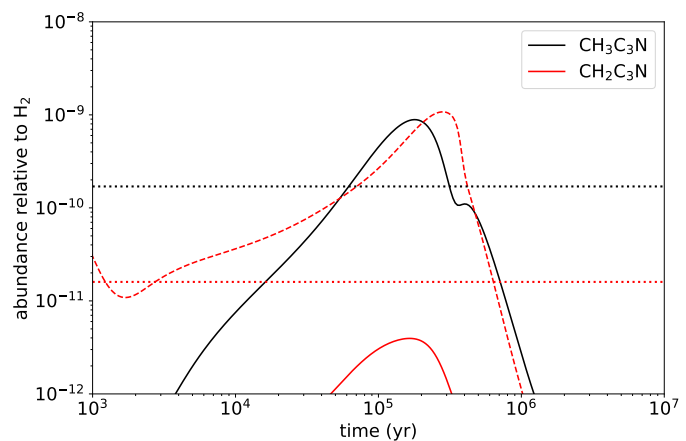


Fig. 4. Calculated fractional abundances of $\text{CH}_3\text{C}_3\text{N}$ and $\text{CH}_2\text{C}_3\text{N}$ as a function of time. The solid red line corresponds to the abundance of $\text{CH}_2\text{C}_3\text{N}$ when the reaction $\text{N} + \text{C}_4\text{H}_3$ is neglected and the dashed red line to the case in which this reaction is included. Horizontal dotted lines correspond to the abundances observed in TMC-1.

s^{-1} in the temperature range 77-296 K (Daugey et al. 2008). Moreover, crossed molecular beam experiments and theoretical calculations indicate that the radical $\text{CH}_2\text{C}_4\text{H}$ is the preferred product, with an estimated branching ratio of 0.65 (Guo et al. 2006b; Mebel et al. 2006). Based on the behaviour of the reaction $\text{C}_2 + \text{CH}_3\text{CCH}$, we adopted a rate coefficient of $3 \times 10^{-10} \text{ cm}^3 \text{ s}^{-1}$ for reaction (2). The radical-radical reactions (3) and (4) have not been studied to our knowledge, although based on the known reactivity of CN and C_3N with unsaturated closed-shell hydrocarbons, it is plausible that they occur with no barrier, yielding $\text{CH}_2\text{C}_3\text{N}$ as one of the main products. We thus adopted a rate coefficient of $10^{-10} \text{ cm}^3 \text{ s}^{-1}$ for them.

We also included an additional formation route to $\text{CH}_2\text{C}_3\text{N}$ through the dissociative recombination of the precursor ion $\text{CH}_3\text{C}_3\text{NH}^+$ with electrons. Loison et al. (2014) estimated a branching ratio of 0.24 for the production of the radical CH_2CN in the dissociative recombination of the smaller analogue ion CH_3CNH^+ , and we thus assumed that the same behaviour holds for the formation of the radical $\text{CH}_2\text{C}_3\text{N}$ in the dissociative recombination of $\text{CH}_3\text{C}_3\text{NH}^+$. The reaction channel of formation of $\text{CH}_2\text{C}_3\text{N}$ then reads



with a rate coefficient of $8 \times 10^{-8} (T/300 \text{ K})^{-0.5} \text{ cm}^3 \text{ s}^{-1}$.

In Fig. 4 we show, as a solid red line, the calculated fractional abundance of $\text{C}_2\text{H}_3\text{CN}$ as a function of time. The peak abundance is about four times lower than the value observed in TMC-1. The main formation routes to $\text{CH}_2\text{C}_3\text{N}$ are reactions (1), (2), (3), and (5), while reaction (4) is only a minor route.

There is another potential formation route to $\text{CH}_2\text{C}_3\text{N}$. In the case of the smaller analogue radical CH_2CN , the chemical model indicates that it is mainly formed through the dissociative recombination of CH_3CNH^+ with electrons, but also by the reaction $\text{N} + \text{C}_2\text{H}_3$, which is known to produce CH_2CN as a main product (Payne et al. 1996). Similarly, it is plausible that the reaction $\text{N} + \text{C}_4\text{H}_3$ yields $\text{CH}_2\text{C}_3\text{N}$. If this reaction is implemented in the chemical model with a rate coefficient similar to that of $\text{N} + \text{C}_2\text{H}_3$, then it becomes the main route to $\text{CH}_2\text{C}_3\text{N}$ and its calculated peak abundance increases by more than two orders of magnitude, lying well above the observed value (see the dashed red line in Fig. 4). However, it is currently not known

whether the reaction $N + C_4H_3$ can produce CH₂C₃N. Moreover, the situation becomes more complicated because there are various possible isomers of the radical C₄H₃, although the chemical network does not distinguish between them. A dedicated study of the reaction $N + C_4H_3$ is needed to shed light on this point.

In Fig. 4 we also show the calculated abundance of the related molecule CH₃C₃N, which has a peak value about five times above the abundance observed in TMC-1. This behaviour is similar to that reported previously in Marcelino et al. (2021).

5. Discussion

In light of the discovery of the radical CH₂C₃N in TMC-1, it is worth comparing its abundance with that of chemically related molecules. In TMC-1 we have $N(CH_2CN) = 1.5 \times 10^{13} \text{ cm}^{-2}$ (Cabezas et al. 2021a), $N(CH_3CN) = 4.7 \times 10^{12} \text{ cm}^{-2}$ (Cabezas et al. 2021a), and $N(CH_3C_3N) = 1.7 \times 10^{12} \text{ cm}^{-2}$ (Marcelino et al. 2021). Therefore, the abundance ratio CH₂C₃N/CH₃C₃N is just 0.09, well below unity. This is in contrast with the smaller analogues, in which case the abundance ratio CH₂CN/CH₃CN is above one, concretely 3.2. This indicates that the chemistry of the cyanides CH₂C₃N and CH₃C₃N behaves differently to that of the smaller analogues CH₂CN and CH₃CN. Moreover, it is unclear whether the radical and the corresponding closed-shell molecule are connected by some common formation routes or have completely disconnected chemistries.

A common route to both CH₂CN and CH₃CN is the dissociative recombination of CH₃CNH⁺. However, the yield ratio CH₂CN/CH₃CN is currently unconstrained (see Vigren et al. 2008). It is likely that this reaction is a major formation pathway to CH₃CN but not to CH₂CN. Even if some CH₂CN is formed during the dissociative recombination of CH₃CNH⁺, most CH₂CN should be formed in TMC-1 through an independent and very efficient process, such as the reaction $N + C_2H_3$. It should be noted that this pathway must be much more efficient than the formation of CH₃CN through CH₃CNH⁺ + e⁻ to account for the higher abundance of CH₂CN compared to CH₃CN and the fact that CH₂CN should be far more reactive than CH₃CN. If true, this implies that the radical C₂H₃ should be abundant in TMC-1.

In the case of the larger cyanides CH₂C₃N and CH₃C₃N, a similar highly efficient route to the radical CH₂C₃N must be prevented since in this case the radical is substantially less abundant than the closed-shell molecule. This takes us to the reaction $N + C_4H_3$, which, according to our chemical model calculations, should not be a major source of CH₂C₃N, unlike in the case of the smaller analogue, where the reaction $N + C_2H_3$ is a major route to CH₂CN. In summary, the routes to the radicals CH₂CN and CH₂C₃N are likely chemically different.

A further point to discuss is whether the radical detected in this work could be an important intermediate to forming larger molecules. Although dedicated studies on the reactivity of CH₂C₃N are needed, our radical could play a role in the synthesis of large organic N-bearing molecules, such as nitrogen heterocycles. For example, benzonitrile (*c*-C₆H₅CN), known to be present in TMC-1 and other molecular clouds (McGuire et al. 2018; Burkhardt et al. 2021) and thought to be formed through the reaction of benzene with CN (Cooke et al. 2020), could be formed through the reaction of CH₂C₃N with allene (CH₂CCH₂), which is suspected to be abundant in TMC-1 (Marcelino et al. 2021; Cernicharo et al. 2021e; Agúndez et al. 2021a).

6. Conclusions

We have reported the detection of the 3-cyano propargyl radical (CH₂C₃N) in the cold dark cloud TMC-1. A total of seven rotational transitions with several hyperfine components were observed in our Q-band TMC-1 survey. This radical is about ten times less abundant than the corresponding closed-shell molecule CH₃C₃N, in contrast to the case of the smaller analogues, where the radical CH₂CN is three times more abundant than CH₃CN. Comparison between the chemical routes of the radicals CH₂CN and CH₂C₃N and the corresponding closed-shell species indicates that the formation routes to the radicals CH₂CN and CH₂C₃N are completely dissimilar.

Acknowledgements. This research has been funded by ERC through grant ERC-2013-Syg-610256-NANOCOSMOS. Authors also thank Ministerio de Ciencia e Innovación for funding support through projects PID2019-106235GB-I00 and PID2019-107115GB-C21 / AEI / 10.13039/501100011033. MA thanks Ministerio de Ciencia e Innovación for grant RyC-2014-16277.

References

- Agúndez, M., & Wakelam, V. 2013, *Chem. Rev.*, 113, 8710
 Agúndez, M., Cernicharo, J., de Vicente, P., et al. 2015, *A&A*, 579, L10
 Agúndez, M., Cabezas, C., Tercero, B., et al. 2021a, *A&A*, 647, L10
 Agúndez, M., Marcelino, N., Tercero, B., et al. 2021b, *A&A*, 649, L4
 Burkhardt, A. M., Loomis, R. A., Shingledecker, C. N., et al. 2021, *Nat Astron.*, 5, 181
 Cabezas, C., Endo, Y., Roueff, E., et al. 2021a, *A&A*, 646, L1
 Cabezas, C., Tercero, B., Agúndez, M., et al. 2021b, *A&A*, 650, L9
 Cabezas, C., Roueff, E., Tercero, B., et al. 2021c, *A&A*, 650, L15
 Chen, W., McCarthy, M. C., Travers, M. J., et al. 1998, *ApJ*, 492, 849
 Cernicharo, J. 1985, Internal IRAM report (Granada: IRAM)
 Cernicharo, J. 2012, in *European Conference on Laboratory Astrophysics*, eds. C. Stehlé, C. Joblin, & L. d'Hendecourt, EAS Publication Series, 58, 251
 Cernicharo, J., Gallego, J. D., López-Pérez, J. A., et al. 2019, *A&A*, 626, A34
 Cernicharo, J., Marcelino, N., Agúndez, M., et al. 2020a, *A&A*, 642, L17
 Cernicharo, J., Marcelino, N., Pardo, J. R., et al. 2020b, *A&A*, 641, L9
 Cernicharo, J., Marcelino, N., Agúndez, M., et al. 2020c, *A&A*, 642, L8
 Cernicharo, J., Cabezas, C., Endo, Y., et al. 2021a, *A&A*, 646, L3
 Cernicharo, J., Cabezas, C., Baillieux, S., et al. 2021b, *A&A*, 646, L7
 Cernicharo, J., Agúndez, M., Kaiser, R., et al. 2021c, *A&A*, 652, L9
 Cernicharo, J., Agúndez, M., Cabezas, C., et al. 2021d, *A&A*, 647, L2
 Cernicharo, J., Cabezas, C., Agúndez, M., et al. 2021e, *A&A*, 647, L3
 Cernicharo, J., Agúndez, M., Cabezas, C., et al. 2021f, *A&A*, 649, L15
 Cernicharo, J., Cabezas, C., Agúndez, M., et al. 2021g, *A&A*, 648, L3
 Cernicharo, J., Cabezas, C., Agúndez, M., et al. 2021h, *A&A*, 650, L14
 Cooke, I. R., Gupta, D., Messenger, J. P., & Sims, I. R. 2020, *ApJ*, 891, L41
 Daugey, N., Caubet, P., Bergeat, A., et al. 2008, *PCCP*, 10, 729
 Guo, Y., Gu, X., Zhang, F., et al. 2006a, *PCCP*, 8, 5454
 Guo, Y., Gu, X., Balucani, N., & Kaiser, R. I. 2006b, *J. Phys. Chem. A*, 110, 6245
 Irvine, W. M., Friberg, P., Hjalmanson, A., et al. 1988, *ApJ*, 334, L107
 Letendre, L., & Dai, H. L., 2002, *J. Phys. Chem. A*, 106, 12035.
 Loison, J.-C., Wakelam, V., & Hickson, K. M. 2014, *MNRAS*, 443, 398
 Marcelino, N., Agúndez, M., Tercero, B., et al. 2020, *A&A*, 643, L6
 Marcelino, N., Tercero, B., Agúndez, M., & Cernicharo, J., 2021, *A&A*, 646, L9
 McElroy, D., Walsh, C., Markwick, A. J., et al. 2013, *A&A*, 550, A36
 McGuire, B. A., Burkhardt, A. M., Kalenskii, S., et al. 2018, *Science*, 359, 202
 Mebel, A. M., Kislov, V. V., & Kaiser, R. I. 2006, *J. Phys. Chem. A*, 110, 2421
 Müller, H. S. P., Schlöder, F., Stutzki, J., & Winnewisser, G. 2005, *J. Mol. Struct.*, 742, 215
 Pardo, J. R., Cernicharo, J., Serabyn, E. 2001, *IEEE Trans. Antennas and Propagation*, 49, 12
 Payne, W. A., Monks, P. S., Nesbitt, F. L., & Stief, L. J. 1996, *J. Chem. Phys.*, 104, 9808
 Prozument, K.; Shaver, R. G.; Ciuba, M. A.; et al. 2013, *Faraday Discuss.* 163, 33.
 Saito, S., Yamamoto, Y., Irvine, W. M., et al., 1988, *ApJ*, 334, L113
 Seiki, K., Sumiyoshi, Y., Oshima, Y., et al. 2000, *Bunshi Kozo Sogo Toronkai Koen Yoshishu*, 2000, 11 (in Japanese).
 Su, H.-F., Kaiser, R. I., & Chang, A. H. H. 2005, *J. Chem. Phys.*, 122, 074320
 Tang, J. Seiki, K., Sumiyoshi, Y., et al. 2000, *The Ohio State 55th International Symposium on Molecular Spectroscopy*, June 12th, 2000
 Tang, J. Sumiyoshi, Y., & Endo, Y., 2001, *ApJ*, 492, 552, 409
 Tercero, F., López-Pérez, J. A., Gallego, J. D., et al., 2021, *A&A* 645, A37
 Vigren, E., Kaminska, M., Hamberg, M., et al. 2008, *PCCP*, 10, 4014